

# Neural Image Space Tessellation

YOUYANG DU, Shandong University, China and Mohamed bin Zayed University of Artificial Intelligence, United Arab Emirates

JUNQIU ZHU, Shandong University, China

ZHENG ZENG, University of California, Santa Barbara, USA

LU WANG\*, Shandong University, China

LINGQI YAN\*, Mohamed bin Zayed University of Artificial Intelligence, United Arab Emirates

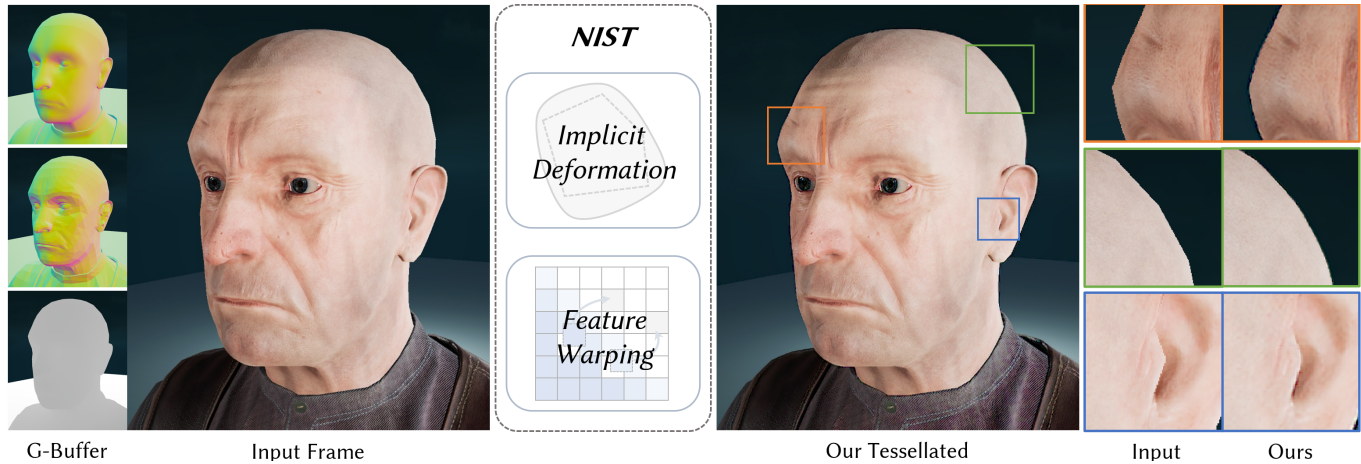


Fig. 1. Our NIST smooths silhouettes directly in screen space using lightweight G-buffer inputs. Without modifying the underlying geometry, our method produces visually smooth and coherent silhouettes comparable to geometric tessellation, as illustrated by the close-up comparisons on the left.

We present Neural Image-Space Tessellation (NIST), a lightweight screen-space post-processing approach that produces the visual effect of tessellated geometry while rendering only the original low-polygon meshes. Inspired by our observation from Phong tessellation, NIST leverages the discrepancy between geometric normals and shading normals as a minimal, view-dependent cue for silhouette refinement. At its core, NIST performs multi-scale neural tessellation by progressively deforming image-space contours with convolutional operators, while jointly reassigning appearance information through an implicit warping mechanism to preserve texture coherence and visual fidelity. Experiments demonstrate that our approach produces smooth, visually coherent silhouettes comparable to geometric tessellation, while incurring a constant per-frame cost and fully decoupled from geometric complexity, making it well-suited for large-scale real-time rendering scenarios. To the best of our knowledge, our NIST is the first work to reformulate tessellation as a post-processing operation, shifting it from a pre-rendering geometry pipeline to a screen space neural post-processing stage.

## 1 INTRODUCTION

The computation workload for modern real-time rendering has been steeply increasing over the last few years. As real-time applications

\*Corresponding authors.

Authors' Contact Information: Youyang Du, Shandong University, Jinan, China and Mohamed bin Zayed University of Artificial Intelligence, Abu Dhabi, United Arab Emirates; Junqiu Zhu, Shandong University, Jinan, China; Zheng Zeng, University of California, Santa Barbara, USA; Lu Wang, Shandong University, Jinan, China; Lingqi Yan, Mohamed bin Zayed University of Artificial Intelligence, Abu Dhabi, United Arab Emirates.

keep pushing toward film-like visual richness, scenes become larger, materials become more complex, and geometric assets are routinely authored at ever higher fidelity. In particular, to avoid close-up geometric artifacts, it is increasingly common to rely on heavy tessellation in the rendering pipeline, which can easily turn otherwise lightweight assets into extremely dense triangle meshes [Boubekeur and Alexa 2008; Catmull and Clark 1978; Loop 1987; Vlachos et al. 2001]. This trend is effective for quality, but it directly translates to higher bandwidth pressure, more expensive rasterization and visibility, and reduced frame rates—especially in scenes with many animated objects and frequent camera close-ups.

The standard solution is to refine geometry explicitly in object space. Tessellation increases geometric resolution, producing smoother silhouettes and higher geometric fidelity. However, object space refinement scales with surface area and scene complexity, and it performs substantial work on geometry that may contribute little to the final image, since the final appearance is inherently view-dependent. This mismatch between object space cost and image space benefit has significantly limited the practical use of high-quality tessellation in large-scale real-time scenes.

In parallel, neural-aided rendering has recently shown a rather consistent pattern of success: instead of making the core rendering pipeline heavier, neural methods are often placed as post-processing modules to reconstruct high-quality appearance from cheaper intermediate results. For example, denoising reduces samples per pixel [Bako et al. 2017; Guo et al. 2019]; spatial upsampling allows

rendering at lower resolution[Xiao et al. 2020; Zhong et al. 2023]; frame interpolation and extrapolation increase temporal sampling without fully rendering every frame[Guo et al. 2021; Wu et al. 2024]. The common theme is to shift expensive computation from pre-rendering or main-pass rendering into a view-dependent image-space post-processing stage, where the cost scales with resolution rather than scene complexity. This observation raises a natural question: *can we move tessellation from the pre-rendering geometry pipeline to a post-rendering screen space stage as well?*

The answer becomes increasingly clear when we realize that silhouette degradation is ultimately perceived in the final rendered image and is inherently view-dependent. This observation motivates a reformulation of silhouette refinement from object space geometry processing into a screen space post-processing problem. From this perspective, the goal is no longer to modify the underlying surface representation, but to improve the perceived continuity of silhouettes in the rendered image. This shift enables silhouette quality to be improved independently of scene complexity, making the approach more suitable for large-scale real-time rendering scenarios.

Based on the above analysis, we present *Neural Image Space Tessellation*, a post-processing approach that produces an image with the visual effect of tessellating the underlying mesh, while rendering only the original low-poly geometry. Our approach is inspired by Phong Tessellation, which seeks a smoothed surface whose geometric normals are consistent with the shading normals implied by the original mesh, achieving visually effective silhouette refinement through small and targeted geometric deformations. While effective, such refinement is traditionally performed as a pre-rendering operation in the rendering pipeline. In contrast, our work explores how this process can be reformulated and moved into a screen-space post-processing stage, where silhouette refinement is performed directly on the rendered image.

However, moving silhouette refinement into screen space raises two key challenges. The first challenge is to determine *where* deformation should be applied in image space. We observe that whether a surface requires refinement under a given view can be inferred from the discrepancy between geometric normals and shading normals: when the two are consistent, no refinement is needed, whereas larger discrepancies directly correlate with silhouette discontinuities. Leveraging this insight, our method operates purely in image space and requires only lightweight G-buffer attributes together with a low-polygon rendered image, without access to high-resolution geometry. The second challenge lies in *how* to perform silhouette refinement in image space. Unlike local appearance filtering or simple pixel-wise mapping, screen-space silhouette refinement entails structured, geometry-like transformations of image content. Traditional convolutional networks struggle with such tasks, as they are poorly suited for modeling large-scale, coherent deformations while preserving high-frequency texture details. To address this challenge, we introduce a multi-scale implicit tessellation strategy in image space. At each scale, refinement is decomposed into two tightly coupled stages handled by dedicated modules: a deformation module that learns contour-aware structural smoothing, and a texture warping module that reconstructs appearance under the inferred deformation. By explicitly separating silhouette continuity from

texture fidelity, our framework enables the network to reason about image-space structural changes while maintaining visual sharpness and seamless texture consistency in the final result. In practice, due to the advantage of our network design, our method achieves nearly constant per-frame overhead across different resolutions, reaching around 6ms at 1080p in our experiments. To the best of our knowledge, this work is the first to explicitly move tessellation from a pre-rendering geometry processing stage into a screen-space post-processing framework.

## 2 RELATED WORK

### 2.1 Traditional Geometric Subdivision and Smoothing

Geometric subdivision techniques, pivotal for enhancing low-poly realism, can be broadly categorized into topology-based global subdivision surfaces and local geometric approximations designed for real-time rendering.

*Subdivision Surfaces.* As the theoretical cornerstone of offline smoothing, the Catmull-Clark algorithm [Catmull and Clark 1978] recursively generates  $C^2$  continuous limit surfaces. For triangular meshes, Loop [1987] introduced the Loop subdivision scheme, a generalization of quartic box-spline surfaces to arbitrary topology, producing  $C^2$  continuous limit surfaces almost everywhere except at extraordinary vertices, where  $C^1$  continuity is maintained. To adapt subdivision surfaces to GPU pipelines, Loop and Schaefer [2008] proposed ACC, which approximates limit surfaces using bi-cubic Bézier patches and decouples tangents to mask geometric seams. Kovacs et al. [2009] extended this approach to handle creases and corners in game-ready models robustly. For scenarios requiring higher precision, Nießner et al. [2012] introduced feature-adaptive subdivision, utilizing pre-computed tables to achieve exact evaluation of RenderMan-quality surfaces on GPUs. Despite their strong theoretical foundations and wide adoption, these subdivision schemes tend to smooth geometry uniformly unless additional constraints are explicitly specified. In practice, this behavior may lead to undesired subdivision effects, such as the smoothing of intentionally sharp geometric features or hard edges that are meant to remain faceted.

*Local Geometric Approximation.* While rigorous, the above subdivision surfaces algorithms incur high overhead due to global topology dependencies. Consequently, “visually smooth” methods relying solely on local information offer a lightweight alternative. PN-Triangles [Vlachos et al. 2001] construct local cubic Bézier surfaces from vertex normals to enhance silhouettes. To address the inherent cracking artifacts, PN-AEN [McDonald and Kilgard 2010] ensures watertight tessellation by introducing edge-adjacency averaging. Alternatively, Phong Tessellation [Boubekeur and Alexa 2008] adopts a minimalist strategy by extending the principle of Phong shading to geometry. For each triangle, its vertices are projected onto planes defined by the corresponding vertex normals, and the final tessellated positions are obtained via barycentric interpolation of these projections. This linear-cost approach favors visual plausibility over strict geometric correctness and was later generalized to arbitrary polygonal meshes by Hettinga and Kosinka [2017].

Unlike these traditional methods that rely heavily on the *Pre-computation Stage* or *Tessellation Stage*—inevitably increasing the number of geometric primitives—our work explores a *screen-space post-processing* solution. We instead apply deep neural networks directly to rendered images exhibiting unsmoothed silhouettes, transforming them into outputs that are perceptually equivalent to those produced from finely tessellated geometry, while completely avoiding the associated geometric complexity overhead.

## 2.2 Neural Postprocessing

*Neural Denoising.* Neural networks have been extensively applied to Monte Carlo denoising as a screen space postprocessing technique, including early learning-based reconstruction [Bako et al. 2017; Chaitanya et al. 2017; Kalantari et al. 2015], quality-driven improvements via loss design, sampling, and adversarial learning [Gharbi et al. 2019; Vogels et al. 2018; Xu et al. 2019], gradient-domain reconstruction [Guo et al. 2019; Kettunen et al. 2019], and more recent approaches incorporating adaptive sampling, feature modeling, and hierarchical or attention-based architectures [Bálint et al. 2023; Chen et al. 2023; Cho et al. 2021; Huo et al. 2020; İşık et al. 2021; Lu et al. 2020; Salehi et al. 2022; Yu et al. 2021].

*Neural Supersampling.* Neural supersampling has been widely studied as a screen-space solution for resolution upscaling and frame generation in real-time rendering, including spatial super-resolution [Xiao et al. 2020; Zhong et al. 2023] and temporal interpolation [Briedis et al. 2021, 2023] or extrapolation [Guo et al. 2021; Wu et al. 2024, 2025] using auxiliary buffers and motion cues. These methods focus on reconstructing missing spatial or temporal samples, rather than modifying image-space geometric structure.

*Generative Neural Post-processing.* Recent work has explored diffusion models for rendering post-processing, enabling flexible re-rendering, appearance editing, and relighting by synthesizing images from rendered inputs or intermediate representations [Liang et al. 2025; Zeng et al. 2025, 2024]. Despite their impressive visual quality, the heavy architectures and iterative sampling processes of diffusion models make them impractical for real-time rendering.

The success of these neural post-processing approaches inspires our exploration of post-processing solutions for tessellation-related effects. However, silhouette refinement requires explicit, structured modifications to image-space content, rather than unconstrained appearance synthesis, and must operate under strict real-time constraints. This motivates our lightweight, contour-aware design based on explicit image-space deformation instead of heavy generative models.

## 3 METHOD

### 3.1 Background and Motivation

Before proceeding, we need to clarify our use of terminology. In the traditional graphics pipeline, tessellation strictly refers to primitive subdivision and does not by itself deform geometry. In practice, however, tessellation is primarily used to enable shape deformation, allowing surfaces to better conform to an intended appearance, such as smoothing. From a perceptual perspective, it is this resulting shape change, rather than the increased triangle count alone, that

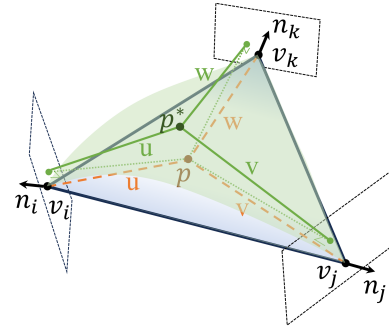


Fig. 2. The illustration of Phong tessellation [Boubekeur and Alexa 2008]. Tessellated points are projected onto planes defined by each vertex and its normal, then barycentrically interpolated and linearly blended with the original position to produce the final displaced point.

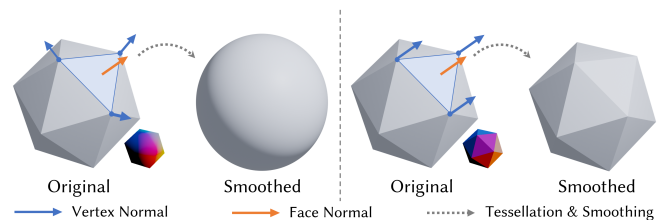


Fig. 3. When shading normals deviate from geometric normals, the implied surface conflicts with the original geometry and requires tessellation for smoothing; conversely, the geometry is already self-consistent, and no smoothing is needed.

improves silhouette quality. Accordingly, we use the term *tessellation* to denote effective silhouette refinement through deformation.

Traditional tessellation techniques address silhouette artifacts by explicitly refining surface geometry in object space. A representative example is *Phong Tessellation*, a lightweight local smoothing scheme that operates on individual triangles. As shown in Figure 2, let a triangle be defined by vertices  $v_i, v_j, v_k$  with corresponding vertex normals  $n_i, n_j, n_k$ . For a point  $p$  inside the triangle, parameterized by barycentric coordinates  $(u, v, w)$ , the projection of  $p$  onto the plane defined by a vertex-normal pair  $(v_*, n_*)$  is given by

$$\pi_*(p) = p - ((p - v_*)^T n_*) n_*, \quad * \in \{i, j, k\}. \quad (1)$$

The displaced position  $p^*$  is obtained by barycentric interpolation of the projected points:

$$p^* = u \cdot \pi_i(p) + v \cdot \pi_j(p) + w \cdot \pi_k(p). \quad (2)$$

Finally, the output vertex position is computed as a linear blend between the original position  $p$  and the deformed position  $p^*$ .

Beyond its practical effectiveness, we find that Phong Tessellation explicitly distinguishes where tessellation is necessary and where it is not. As shown in Figure 3, by examining the discrepancy between shading normals and geometric normals, the method selectively applies refinement only in regions that require it, while leaving already

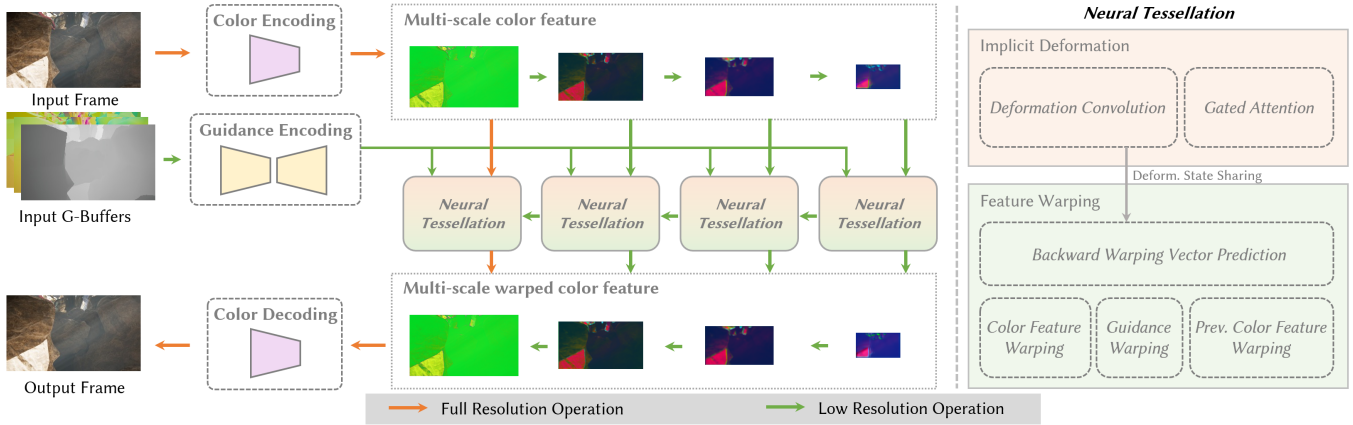


Fig. 4. Overview of the NIST pipeline. The left part illustrates the overall workflow: given an input frame and standard G-buffer inputs, color and guidance features are encoded and processed through a multi-scale neural tessellation pipeline before being decoded into the final output. The right part shows the internal structure of the neural tessellation module. Most computations in NIST are performed at reduced resolutions, while only the first-level color feature processing is carried out at full resolution to maximize the preservation of fine image details.

coherent areas unchanged. This normal-based criterion avoids unnecessary deformation and leads to smooth silhouettes that remain visually natural and consistent with the intended appearance.

Unlike prior work that treats silhouette artifacts purely as a geometry refinement problem, we reinterpret them as a screen-space perceptual inconsistency. Specifically, shading across a surface appears smooth, yet this perceptual smoothness is abruptly broken by geometric discontinuities at silhouettes. Resolving this inconsistency often requires only small, structured deformations in image space to align silhouettes with the appearance implied by shading, while newly exposed regions can be reconstructed from existing image space content. Together, these observations suggest that silhouette refinement is well-suited to be formulated as a screen space post-processing task.

### 3.2 Overview of NIST

We formulate Neural Image-Space Tessellation (NIST) as a screen-space post-processing problem that aims to resolve visual perceptual inconsistencies in rendered images. Given an input rendering that exhibits coarse silhouettes due to low geometric resolution, together with a small set of auxiliary G-buffers, NIST directly outputs an image with perceptually smooth silhouettes, without modifying the underlying mesh or increasing geometric complexity. Concretely, the input to NIST consists of the original rendered image, a depth buffer, a geometric normal buffer, and a shading normal buffer. These signals jointly provide sufficient guidance for the network to infer where and how silhouettes should be deformed in image space. The network operates end-to-end, producing a final image in which perceptual inconsistencies are resolved, and silhouette continuity is improved while preserving texture fidelity and overall visual coherence.

A key advantage of our formulation is that all required inputs are easily acquired in modern real-time rendering pipelines. Both normals are inexpensive to compute and are commonly stored in

G-buffers. In addition, we incorporate a depth buffer, which provides relative geometric ordering and explicit cues about visibility and silhouette formation in screen space.

Throughout this paper, we use the terms *image space* and *screen space* interchangeably. To follow common conventions, we adopt the term *screen space* when discussing rendering pipeline concepts and operations, and use *image space* when referring to neural network processing and learning-based formulations. Both terms denote computations performed in the 2D domain of the rendered image.

### 3.3 Network Architecture

An overview of the NIST framework is shown in Figure 4. NIST performs multi-scale neural tessellation in screen space, progressively refining silhouettes by applying image-space displacements to color features at multiple resolutions.

At each scale, a single neural tessellation step is decomposed into two conceptually distinct processes. The first process determines how the image-space geometry should be deformed, i.e., where new contour regions should emerge after deformation. The second process determines how appearance information should be re-assigned to the deformed image space in order to preserve texture fidelity. Correspondingly, we design two specialized modules to address these challenges: an *Implicit Deformation Module*, which infers contour-aware structural deformation in image space, and a *feature Warping Module*, which reconstructs appearance under the inferred deformation.

The multi-scale design serves a dual purpose. At lower resolutions, neural tessellation captures large-scale, coherent image-space deformations that establish the overall silhouette structure. At higher resolutions, it performs localized, fine-grained refinements to ensure smooth and visually consistent contours. Through the cooperative effect of neural tessellation across scales, NIST produces smooth

silhouette transitions that resemble the visual outcome of geometric tessellation, while operating entirely in screen space. We next describe the two core modules in detail.

*Implicit Deformation Module.* The Implicit Deformation Module is responsible for inferring structured, contour-aware image-space deformation at each scale. To this end, the module maintains an implicit deformation state  $z_d^{(t)}$ , which encodes the information required to perform neural tessellation at scale  $t$ .

A key design choice is that tessellation-related deformation depends solely on geometric cues rather than rendered color. This observation is reflected in our architecture. Specifically, we first encode a set of auxiliary geometry buffers—geometric normals (i.e., face normals), shading normals (i.e., interpolated vertex normals), and depth—into a tessellation guidance feature  $z_g$ . The guidance feature  $z_g$  modulates the deformation state through an attention mechanism based on gated convolutions. At each scale, we compute query, key, and value features as

$$Q = F_q(z_g^{(t-1)}), \quad K = F_k(z_*^{(t-1)}), \quad V = F_v(z_*^{(t-1)}), \quad (3)$$

where  $z_* = z_g$  for  $t = 1$ , initializing the deformation state via self-attention over the guidance features, and  $z_* = z_d$  for  $t \neq 1$ , enabling cross-scale propagation of deformation information. The attended deformation state is then computed as

$$z_d^{(t-1)} = \text{Softmax}(F_a(Q, K)) \cdot V. \quad (4)$$

This design is motivated by the empirical observation that modulating convolutional feature responses can induce structured changes in feature geometry, allowing the network to represent contour deformation implicitly. The updated deformation state is subsequently refined by a dedicated Deformation Block, which explicitly reshapes the contour structure encoded in the deformation state:

$$z_d^{(t)} = \text{Deform}(z_d^{(t-1)}). \quad (5)$$

*Feature Warping Module.* Image-space deformation inevitably alters the spatial arrangement of appearance information. To preserve high-frequency texture details under deformation, we introduce a dedicated Feature Warping Module. This design is based on the assumption that, after tessellation, newly exposed or displaced regions can be reconstructed from existing image-space content rather than synthesized from scratch.

Given the deformation state  $z_d^{(t)}$ , the Feature Warping Module predicts a backward warping vector field  $v^{(t)}$  that defines the pixel-wise correspondence between the deformed and original image spaces:

$$v^{(t)} = \tanh(F_w(z_d^{(t)})). \quad (6)$$

This warping field is applied to the color features propagated from the previous scale, denoted  $\hat{z}_c^{(t-1)}$ , as well as to the guidance features  $z_g^{(t-1)}$ . Warping the guidance features ensures that geometric cues remain spatially aligned with the deformation state, preventing contour mismatches that could lead to erroneous refinement.

In addition, color features  $z_c^{(t)}$  extracted at the current scale from the encoder have not undergone any prior deformation. Since the predicted warping vector  $v^{(t)}$  is defined relative to the previous

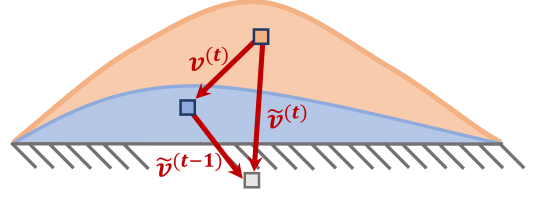


Fig. 5. Under multi-level backward warping, the final warp vector  $\tilde{v}^{(t)}$  pointing to the original pixel location is obtained by accumulating the historical warping vectors across all levels.

scale, we maintain a cumulative warping vector  $\tilde{v}^{(t)}$  to account for the full deformation history:

$$\tilde{v}^{(t)} = v^{(t)} + \tilde{v}^{(t-1)}. \quad (7)$$

The complete warping process is given by

$$z_g^{(t)} = \text{Warp}(z_g^{(t-1)}, v^{(t)}), \quad (8)$$

$$\hat{z}_c^{(t-1)} = \text{Warp}(\hat{z}_c^{(t-1)}, v^{(t)}), \quad (9)$$

$$z_c^{(t)} = \text{Warp}(z_c^{(t)}, \tilde{v}^{(t)}). \quad (10)$$

The warped color features from the previous scale  $\hat{z}_c^{(t-1)}$  and the warped encoder features  $z_c^{(t)}$  are then concatenated to produce the refined color feature  $\hat{z}_c^{(t)}$ , which is passed to the next scale for further neural tessellation.

### 3.4 Loss Function

We train NIST using a composite loss function designed to jointly supervise contour deformation accuracy and appearance fidelity. The overall loss consists of three complementary terms, each targeting a distinct aspect of the neural tessellation process.

The primary loss encourages accurate refinement in regions affected by image-space deformation. Rather than directly penalizing absolute differences between the predicted image  $I^{pred}$  and the ground-truth image  $I^{label}$ , we adopt a residual-relative formulation that emphasizes discrepancies relative to the input rendering  $I^{input}$ . This design strengthens supervision in regions where tessellation induces meaningful changes while down-weighting areas that remain largely unchanged. The loss is defined as

$$\mathcal{L}_{RR} = \frac{1}{N} \sum_i \frac{|I_i^{pred} - I_i^{label}|}{|I_i^{label} - I_i^{input}| + \epsilon}, \quad (11)$$

where  $N$  denotes the number of pixels in the image and  $\epsilon = 10^{-6}$  is a small constant for numerical stability.

To further improve silhouette accuracy, we incorporate a shading-augmented loss inspired by Guo et al. [2021]. This term penalizes pixels with large prediction errors by explicitly focusing on the  $k$  pixels exhibiting the highest residuals. Since inaccurate deformation typically manifests as pronounced pixel-wise discrepancies near silhouettes, this loss effectively emphasizes regions where contour

misalignment occurs. The loss is defined as

$$\mathcal{L}_{shade} = \frac{1}{k} \sum_{i \in S_k} |I_i^{pred} - I_i^{label}|, \quad (12)$$

where  $S_k$  denotes the set of indices corresponding to the  $k$  pixels with the largest prediction errors.

While the deformation-related losses guide silhouette refinement, they alone are insufficient to ensure faithful reconstruction of fine-scale texture details. To preserve high-frequency appearance and prevent over-smoothed outputs, we additionally employ the LPIPS [Zhang et al. 2018], denoted as  $\mathcal{L}_{LPIPS}$ , which encourages perceptual similarity between the predicted and ground-truth images in a learned feature space.

The final training loss function is a weighted combination of the three loss terms:

$$\mathcal{L} = \lambda_{RR} \mathcal{L}_{RR} + \lambda_{shade} \mathcal{L}_{shade} + \lambda_{LPIPS} \mathcal{L}_{LPIPS}. \quad (13)$$

In all experiments, we set  $\lambda_{RR} = 0.1$ ,  $\lambda_{shade} = 10$ , and  $\lambda_{LPIPS} = 30$ .

### 3.5 Implementation Details

To improve generalization across viewpoints, we transform both geometric normals and shading normals into camera space before feeding them into the network. Although the input and output images share large overlapping regions, we directly predict the final rendered result rather than learning a residual formulation. We make this choice because our feature warping globally reassigns color features across the image space, including newly formed regions introduced by deformation, rather than only applying localized corrections to the input. Since silhouette smoothing primarily involves low-frequency structural changes, all deformation and feature warping operations are performed at a reduced resolution (360p), while only the first-level color feature processing is carried out at full resolution to preserve fine appearance details. This design significantly reduces computational cost without compromising visual quality.

Our network is implemented in PyTorch and optimized using Adam with a learning rate of  $1 \times 10^{-4}$  and a weight decay of  $1 \times 10^{-5}$ . Unless otherwise specified, all learnable mappings in our network are implemented using a Double Convolution block consisting of two  $3 \times 3$  convolutional layers with a LeakyReLU activation in between. The only exception is the Deform Block, whose first convolution uses a  $7 \times 7$  kernel to increase the receptive field and better capture large-scale, structured contour deformations. All models are trained on a single NVIDIA A100 GPU with a batch size of 4 for approximately 24 hours.

## 4 RESULTS AND COMPARISONS

To evaluate the effectiveness of our NIST, we compare our method against a representative traditional tessellation approach. Specifically, we use the PN-Triangles [Vlachos et al. 2001] algorithm as implemented in Unreal Engine 4.27 as our reference. Our evaluation is conducted on four scenes in total: three scenes are split into disjoint training and testing sets, while the remaining scene is used exclusively for testing to assess generalization, as shown in Table 1. In addition to comparisons with traditional methods, we perform a series of ablation studies to analyze the key components of our

Table 1. Dataset statistics for the evaluated scenes. We report the number of training and testing frames, as well as the maximum number of visible mesh faces per frame.

Scene	Training Set	Testing Set	Max. Visible Faces
JUNKYARD	0	1000	39,621K
SOULCAVE	4000	540	584.4K
COWBOY	2500	500	462.2K
BRONZE	3000	500	780.4K

Table 2. Inference latency breakdown (mean, in ms) at different input resolutions.

Resolution	H2D	GPU Compute	D2H	Total
360p	0.145	<b>4.520</b>	0.034	<b>4.699</b>
720p	0.537	<b>5.000</b>	0.136	<b>5.673</b>
1080p	1.190	<b>6.186</b>	0.304	<b>7.680</b>

framework. All experiments are executed on a desktop PC equipped with an Intel i9-14900K CPU and an NVIDIA RTX 5090 GPU.

### 4.1 Qualitative and Quantitative Comparison

Figure 7 presents qualitative comparisons between our method and traditional tessellation across four representative scenes. For each scene, we show the original input rendering without any silhouette smoothing, the result produced by PN-Triangles as implemented in Unreal Engine 4.27, and the output of NIST. In addition, two representative regions are highlighted and magnified for each frame to facilitate close inspection of silhouette quality and local surface continuity.

Across all scenes, NIST effectively removes visually distracting silhouette artifacts present in the unsmoothed input, producing results that closely resemble those obtained with geometric tessellation. In scenes such as SOULCAVE, which exhibit large-scale geometric deformation, NIST successfully performs substantial image-space contour refinement, recovering smooth and coherent outlines without introducing visible distortions. In contrast, scenes featuring organic surfaces, such as COWBOY, benefit from NIST’s ability to perform subtle, fine-grained smoothing, resulting in visually consistent silhouettes that preserve the original appearance. The zoomed-in regions further demonstrate that NIST maintains high-frequency appearance details and produces seamless transitions along refined contours, despite operating entirely in screen space.

We also observe that NIST is able to avoid unnecessary smoothing in regions where geometric normals and shading normals are consistent. Figure 9 shows an additional example from the JUNKYARD scene, where straight structural elements are preserved by our method, while PN-Triangles introduces undesired deformation despite the absence of perceptual inconsistency. This behavior highlights the effectiveness of our normal-based guidance in selectively applying deformation only where refinement is required.

### 4.2 Resolution Scaling and Performance

To evaluate the scalability of NIST with respect to image resolution, we report its inference performance under different rendering

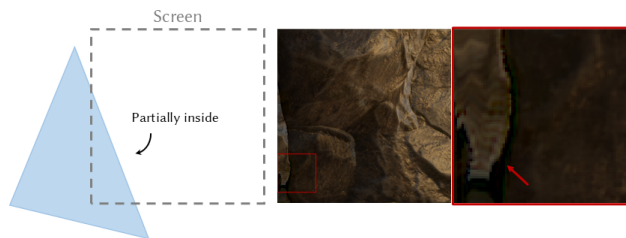


Fig. 6. Screen space artifacts caused by partially visible triangles. In this case, incomplete geometric information may lead to unstable image space deformation and visible artifacts.

resolutions. Table 2 summarizes the inference latency measured at 360p, 720p, and 1080p in a representative scene. As shown in the table, the inference cost of NIST increases modestly with image resolution instead of a linear increment. Importantly, this cost is independent of scene geometric complexity, in contrast to geometry-based tessellation methods whose performance scales with mesh complexity.

### 4.3 Ablation Study

We conduct ablation studies to evaluate the contribution of three key components in NIST: the implicit deformation module, the texture warping module, and the LPIPS perceptual loss. The results are shown in Figure 8.

When the implicit deformation module is removed and replaced with an equivalent lightweight  $3 \times 3$  convolution, the network fails to learn meaningful image-space deformation, resulting in silhouettes that remain largely unchanged from the input. Removing the feature warping module leads to visible seams between deformed and original regions, and the newly formed areas exhibit noticeable loss of appearance fidelity. Finally, when LPIPS is excluded from the training objective, the deformed regions become overly smooth and lack high-frequency details, producing visually blurred results. These ablations demonstrate that our implicit image space deformation, explicit feature warping-based reassignment, and perceptual supervision are all essential for achieving coherent and high-fidelity image space tessellation.

### 4.4 Discussion and Limitations

*Generality.* Our current framework is primarily trained in a per-scene manner, similar to early neural post-processing approaches (e.g., ExtraNet [Guo et al. 2021] and DLSS 1.0 [Edelsten et al. 2019]). However, we observe that when trained on a mixture of multiple scenes, the network can generalize to previously unseen scenes with acceptable visual quality, as the JUNKYARD shown in Figure 7. While this generalization is not yet sufficient to support fully scene-agnostic deployment, it suggests that the learned image-space tessellation behavior is not strictly tied to a single scene configuration.

*Screen Space Limitations.* As a screen space method, NIST inherits limitations related to incomplete visibility. First, when only partial geometry of a triangle is visible in screen space, the inferred

deformation may become unstable near boundaries. Second, deformations corresponding to completely invisible geometry cannot be expressed in screen space and therefore do not contribute to the final result. Figure 6 shows the potential artifacts caused by the incomplete screen space triangles. These limitations are inherent to screen space formulations and reflect the trade-off between geometric completeness and postprocessing efficiency.

*Performance.* Our current implementation does not incorporate industrial-level optimizations such as quantization. Nevertheless, due to the advantage of our framework design, the inference cost remains nearly constant across different resolutions, as shown in Table 2, and is decoupled from scene geometric complexity. This behavior contrasts with traditional tessellation pipelines whose cost scales with geometric complexity, and demonstrates the efficiency advantage of our approach even without aggressive optimization.

*Quality.* NIST is not designed to reproduce reference tessellation results on a per-pixel alignment. Instead, its goal is to eliminate perceptual inconsistencies introduced by coarse geometry. While subtle differences from geometry-based references may remain, the resulting images exhibit smooth and coherent silhouettes that are visually comparable for real-time rendering applications.

*Shading Normals.* In our current formulation, we use interpolated vertex normals as shading normals and do not incorporate normal maps. This design choice reflects our focus on geometric smoothing rather than adding fine-scale surface detail. Extending the framework to jointly handle silhouette smoothing and detail enhancement under a unified formulation remains a promising direction for future work.

*Geometric Normals vs. Depth.* In principle, depth information alone could be used to infer geometric normal in screen space. However, our experiments show that explicitly providing geometric face normals significantly improves learning stability and deformation accuracy. As a result, we include both depth and geometric normal buffers as inputs, leveraging their complementary strengths for guiding image-space tessellation.

## 5 CONCLUSION AND FUTURE WORK

We have presented Neural Image-Space Tessellation, a lightweight screen-space post-processing approach that reformulates tessellation from an object-space geometry refinement task into an image-space perceptual problem. By leveraging the discrepancy between geometric face normals and interpolated vertex normals as a minimal, view-dependent cue, NIST performs multi-scale neural tessellation through structured image-space deformation while preserving appearance fidelity via feature warping. This design decouples silhouette smoothness from geometric complexity and enables silhouette refinement whose cost scales with image resolution rather than scene detail. Experimental results demonstrate that NIST produces smooth, visually coherent silhouettes comparable to those obtained with geometric tessellation, while avoiding its associated computational overhead. In particular, our method maintains nearly constant per-frame cost across different input resolutions, with

inference time remaining around 6 ms even at the highest tested resolution of 1080p.

Several directions remain open for future work. Model compression techniques such as distillation and quantization could further reduce inference, while training on larger and more diverse datasets may improve generalization across scenes and materials. In addition, incorporating explicit temporal modeling through sequence-based training could further enhance temporal stability in dynamic scenes.

## References

- Steve Bako, Thijs Vogels, Brian McWilliams, Mark Meyer, Jan Novák, Alex Harvill, Pradeep Sen, Tony DeRose, and Fabrice Rousselle. 2017. Kernel-predicting convolutional networks for denoising Monte Carlo renderings. *ACM Transactions on Graphics (TOG)* 36 (2017), 1–14. <https://api.semanticscholar.org/CorpusID:31004998>
- Martin Bálint, Krzysztof Wolski, Karol Myszkowski, Hans-Peter Seidel, and Rafal K. Mantiuk. 2023. Neural Partitioning Pyramids for Denoising Monte Carlo Renderings. *ACM SIGGRAPH 2023 Conference Proceedings* (2023). <https://api.semanticscholar.org/CorpusID:259644461>
- Tamy Boubekeur and Marc Alexa. 2008. Phong Tessellation. *ACM Trans. Graph.* 27 (2008), 141. <https://api.semanticscholar.org/CorpusID:6502335>
- Karlis Martins Briedis, Abdelaziz Djelouah, Mark Meyer, Ian McGonigal, Markus H. Gross, and Christopher Schroers. 2021. Neural frame interpolation for rendered content. *ACM Transactions on Graphics (TOG)* 40 (2021), 1–13. <https://api.semanticscholar.org/CorpusID:245014001>
- Karlis Martins Briedis, Abdelaziz Djelouah, Raphael Ortiz, Mark Meyer, Markus H. Gross, and Christopher Schroers. 2023. Kernel-Based Frame Interpolation for Spatio-Temporally Adaptive Rendering. *ACM SIGGRAPH 2023 Conference Proceedings* (2023). <https://api.semanticscholar.org/CorpusID:259975910>
- E. Catmull and J. Clark. 1978. Recursively generated B-spline surfaces on arbitrary topological meshes. *Computer-Aided Design* 10, 6 (1978), 350–355. [doi:10.1016/0010-4485\(78\)90110-0](https://doi.org/10.1016/0010-4485(78)90110-0)
- Chakravarty Reddy Alla Chaitanya, Anton Kaplanyan, Christoph Schied, Marco Salvi, Aaron E. Lefohn, Derek Nowrouzezahrai, and Timo Aila. 2017. Interactive reconstruction of Monte Carlo image sequences using a recurrent denoising autoencoder. *ACM Transactions on Graphics (TOG)* 36 (2017), 1–12. <https://api.semanticscholar.org/CorpusID:3350221>
- Bingyi Chen, Zengyu Liu, Li Yuan, Zhitao Liu, Yi Li, Guan Wang, and Ning Xie. 2023. Monte Carlo Denoising via Multi-scale Auxiliary Feature Fusion Guided Transformer. *SIGGRAPH Asia 2023 Technical Communications* (2023). <https://api.semanticscholar.org/CorpusID:265450029>
- I Cho, Yuchi Huo, and Sung eui Yoon. 2021. Weakly-supervised contrastive learning in path manifold for Monte Carlo image reconstruction. *ACM Transactions on Graphics (TOG)* 40 (2021), 1–14. <https://api.semanticscholar.org/CorpusID:236004240>
- Andrew Edelsten, Paula Jukarainen, and Anjul Patney. 2019. Truly Next-Gen: Adding Deep Learning to Games and Graphics. Game Developers Conference (GDC), NVIDIA Sponsored Session. Presented in the Programming Track.
- Michaël Gharbi, Tzu-Mao Li, Miika Aittala, Jaakko Lehtinen, and Frédo Durand. 2019. Sample-based Monte Carlo denoising using a kernel-splating network. *ACM Transactions on Graphics (TOG)* 38 (2019), 1–12. <https://api.semanticscholar.org/CorpusID:196834663>
- Jie Guo, Xihao Fu, Liqiang Lin, Hengjun Ma, Yanwen Guo, Shiqiu Liu, and Ling-Qi Yan. 2021. ExtraNet: real-time extrapolated rendering for low-latency temporal supersampling. *ACM Transactions on Graphics (TOG)* 40 (2021), 1–16. <https://api.semanticscholar.org/CorpusID:237510662>
- Jie Guo, Mengtian Li, Quewei Li, Yuting Qiang, Bingyang Hu, Yanwen Guo, and Ling-Qi Yan. 2019. GradNet. *ACM Transactions on Graphics (TOG)* 38 (2019), 1–13. <https://api.semanticscholar.org/CorpusID:202754826>
- Gerben Jan Hetinga and Jiri Kosinka. 2017. Phong Tessellation and PN Polygons for Polygonal Models. In *Eurographics*. <https://api.semanticscholar.org/CorpusID:46910267>
- Yuchi Huo, Rui Wang, Ruzahng Zheng, Huali Xu, Hujun Bao, and Sung eui Yoon. 2020. Adaptive Incident Radiance Field Sampling and Reconstruction Using Deep Reinforcement Learning. *ACM Transactions on Graphics (TOG)* 39 (2020), 1–17. <https://api.semanticscholar.org/CorpusID:211536743>
- Mustafa Serkan İşik, Matthew Fisher, Jonathan Eisenmann, and Michaël Gharbi. 2021. Interactive Monte Carlo denoising using affinity of neural features. *ACM Transactions on Graphics (TOG)* 40 (2021), 1–13. <https://api.semanticscholar.org/CorpusID:235128595>
- Nima Khademi Kalantari, Steve Bako, and Pradeep Sen. 2015. A machine learning approach for filtering Monte Carlo noise. *ACM Transactions on Graphics (TOG)* 34 (2015), 1–12. <https://api.semanticscholar.org/CorpusID:15982571>
- Markus Kettunen, Erik Härkönen, and Jaakko Lehtinen. 2019. Deep convolutional reconstruction for gradient-domain rendering. *ACM Transactions on Graphics (TOG)* 38 (2019), 1–12. <https://api.semanticscholar.org/CorpusID:196834602>
- Denis Kovacs, Jason Mitchell, Shanon Drone, and Denis Zorin. 2009. Real-time creased approximate subdivision surfaces. In *Proceedings of the 2009 Symposium on Interactive 3D Graphics and Games* (Boston, Massachusetts) (*I3D '09*). Association for Computing Machinery, New York, NY, USA, 155–160. [doi:10.1145/1507149.1507174](https://doi.org/10.1145/1507149.1507174)
- Ruofan Liang, Zan Gojic, Huan Ling, Jacob Munkberg, Jon Hasselgren, Zhi-Hao Lin, Jun Gao, Alexander Keller, Nandita Vijaykumar, Sanja Fidler, and Zian Wang. 2025. DiffusionRenderer: Neural Inverse and Forward Rendering with Video Diffusion Models. *2025 IEEE/CVF Conference on Computer Vision and Pattern Recognition (CVPR)* (2025), 26069–26080. <https://api.semanticscholar.org/CorpusID:275993796>
- Charles T. Loop. 1987. Smooth Subdivision Surfaces Based on Triangles. <https://api.semanticscholar.org/CorpusID:116150707>
- Charles T. Loop and Scott Schaefer. 2008. Approximating Catmull-Clark subdivision surfaces with bicubic patches. *ACM Trans. Graph.* 27 (2008), 8:1–8:11. <https://api.semanticscholar.org/CorpusID:6068564>
- Yifan Lu, Ning Xie, and Heng Tao Shen. 2020. DMCR-GAN: Adversarial Denoising for Monte Carlo Renderings with Residual Attention Networks and Hierarchical Features Modulation of Auxiliary Buffers. *SIGGRAPH Asia 2020 Technical Communications* (2020). <https://api.semanticscholar.org/CorpusID:227129200>
- John McDonald and Mark Kilgard. 2010. *Crack-Free Point-Normal Triangles Using Adjacent Edge Normals*. White Paper WP-05621-001, NVIDIA Corporation. <https://developer.download.nvidia.com/whitepapers/2010/PN-AEN-Triangles-Whitepaper.pdf>
- Matthias Nießner, Charles Loop, Mark Meyer, and Tony DeRose. 2012. Feature-adaptive GPU rendering of Catmull-Clark subdivision surfaces. *ACM Trans. Graph.* 31, 1, Article 6 (Feb. 2012), 11 pages. [doi:10.1145/2077341.2077347](https://doi.org/10.1145/2077341.2077347)
- Farnood Salehi, Marco Manzi, Gerhard Roethlin, Romann M. Weber, Christopher Schroers, and Marios Pappas. 2022. Deep Adaptive Sampling and Reconstruction Using Analytic Distributions. *ACM Transactions on Graphics (TOG)* 41 (2022), 1–16. <https://api.semanticscholar.org/CorpusID:254097248>
- Alex Vlachos, Jörg Peters, Chas. Boyd, and Jason L. Mitchell. 2001. Curved PN triangles. In *ACM Symposium on Interactive 3D Graphics and Games*. <https://api.semanticscholar.org/CorpusID:5227025>
- Thijs Vogels, Fabrice Rousselle, Brian McWilliams, Gerhard Röthlin, Alex Harvill, David Adler, Mark Meyer, and Jan Novák. 2018. Denoising with kernel prediction and asymmetric loss functions. *ACM Transactions on Graphics (TOG)* 37 (2018), 1–15. <https://api.semanticscholar.org/CorpusID:46891159>
- Songyin Wu, Deepak Vembar, Anton Sochenov, Selvakumar Panneer, Sungye Kim, Anton Kaplanyan, and Ling-Qi Yan. 2024. GFEE: G-buffer Free Frame Extrapolation for Low-latency Real-time Rendering. *ACM Transactions on Graphics (TOG)* 43 (2024), 1–15. <https://api.semanticscholar.org/CorpusID:270764543>
- Zhizhen Wu, Zhilong Yuan, Chenyu Zuo, Yazhen Yuan, Yifan Peng, Guiyang Pu, Rui Wang, and Yuchi Huo. 2025. MoFlow: Motion-Guided Flows for Recurrent Rendered Frame Prediction. *ACM Transactions on Graphics* 44 (2025), 1–18. <https://api.semanticscholar.org/CorpusID:277936830>
- Lei Xiao, Salah Nouri, Matthew Chapman, Alexander Fix, Douglas Lanman, and Anton Kaplanyan. 2020. Neural supersampling for real-time rendering. *ACM Transactions on Graphics (TOG)* 39 (2020), 142:1–142:12. <https://api.semanticscholar.org/CorpusID:221105079>
- Bing Xu, J. Zhang, Rui Wang, Kun Xu, Yong-Liang Yang, Chuan Li, and Rui Tang. 2019. Adversarial Monte Carlo denoising with conditioned auxiliary feature modulation. *ACM Transactions on Graphics (TOG)* 38 (2019), 1–12. <https://api.semanticscholar.org/CorpusID:203082682>
- Jiaqi Yu, Yongwei Nie, Chengjiang Long, Wenju Xu, Qing Zhang, and Guiqing Li. 2021. Monte Carlo denoising via auxiliary feature guided self-attention. *ACM Transactions on Graphics (TOG)* 40 (2021), 1–13. <https://api.semanticscholar.org/CorpusID:244728216>
- Yu Zeng, Charles Ochoa, Mingyuan Zhou, Vishal M. Patel, Vitor Guizilimi, and Rowan McAllister. 2025. NeuralRemaster: Phase-Preserving Diffusion for Structure-Aligned Generation. <https://api.semanticscholar.org/CorpusID:283556775>
- Zheng Zeng, Valentin Deschaintre, Iliyan Georgiev, Yannick Hold-Geoffroy, Yiwei Hu, Fujun Luan, Ling-Qi Yan, and Miloš Hašan. 2024. RGBX: Image decomposition and synthesis using material- and lighting-aware diffusion models. *ACM SIGGRAPH 2024 Conference Papers* (2024). <https://api.semanticscholar.org/CorpusID:269484178>
- Richard Zhang, Phillip Isola, Alexei A. Efros, Eli Shechtman, and Oliver Wang. 2018. The Unreasonable Effectiveness of Deep Features as a Perceptual Metric. arXiv:1801.03924 [cs.CV] <https://arxiv.org/abs/1801.03924>
- Zhihua Zhong, Jingsen Zhu, Yuxin Dai, Chuankun Zheng, Guanlin Chen, Yuchi Huo, Hujun Bao, and Rui Wang. 2023. FuseSR: Super Resolution for Real-time Rendering through Efficient Multi-resolution Fusion. *SIGGRAPH Asia 2023 Conference Papers* (2023). <https://api.semanticscholar.org/CorpusID:264146553>

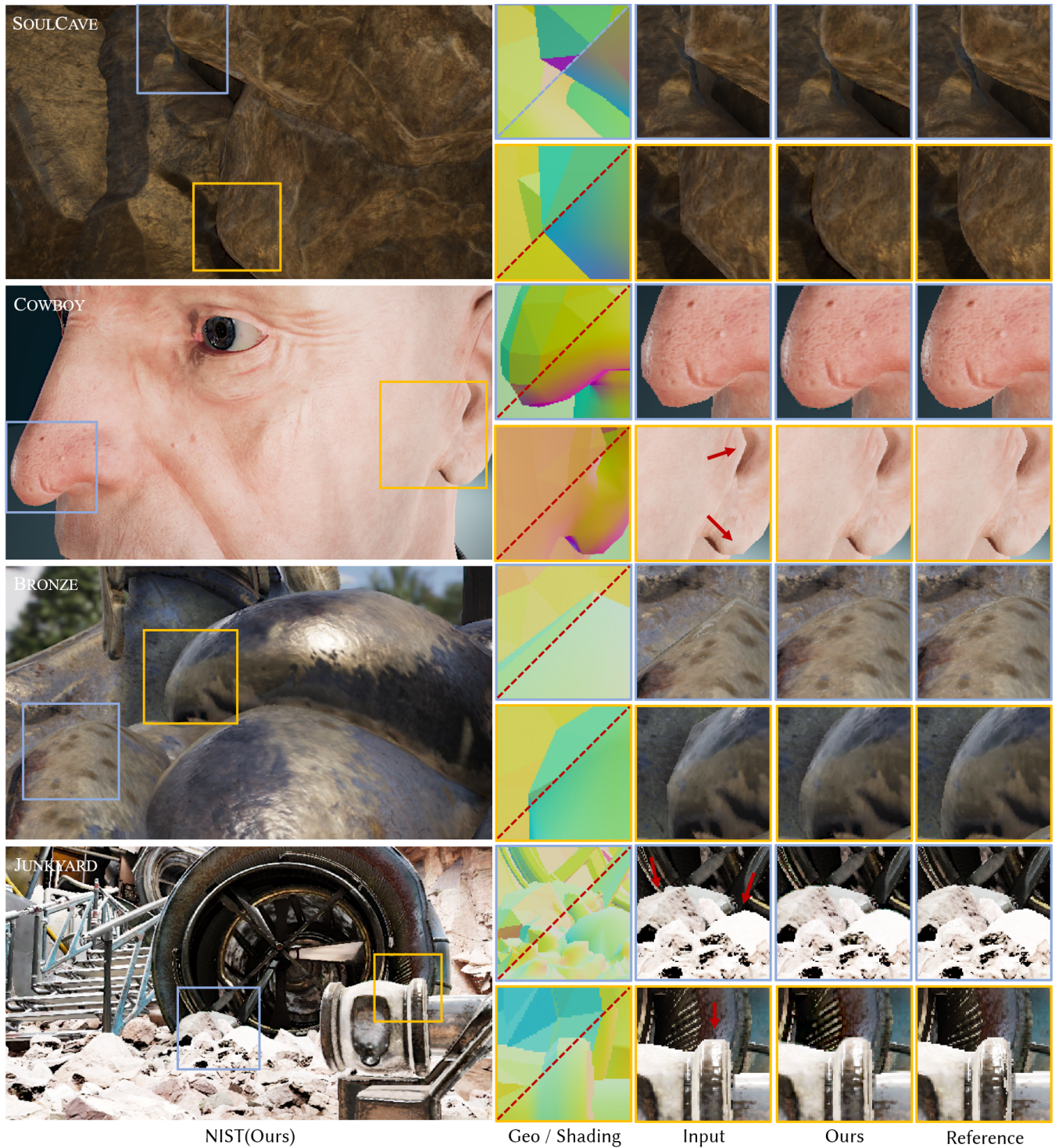


Fig. 7. Qualitative comparison across four scenes. From top to bottom: SOULCAVE, COWBOY, BRONZE, and JUNKYARD. The left column shows the output of NIST. For each scene, two representative regions are highlighted and magnified on the right, comparing the input rendering, our result, and the reference. We also show the geometric normals and shading normals in the middle. NIST effectively removes silhouette artifacts while producing results visually comparable to geometric tessellation.

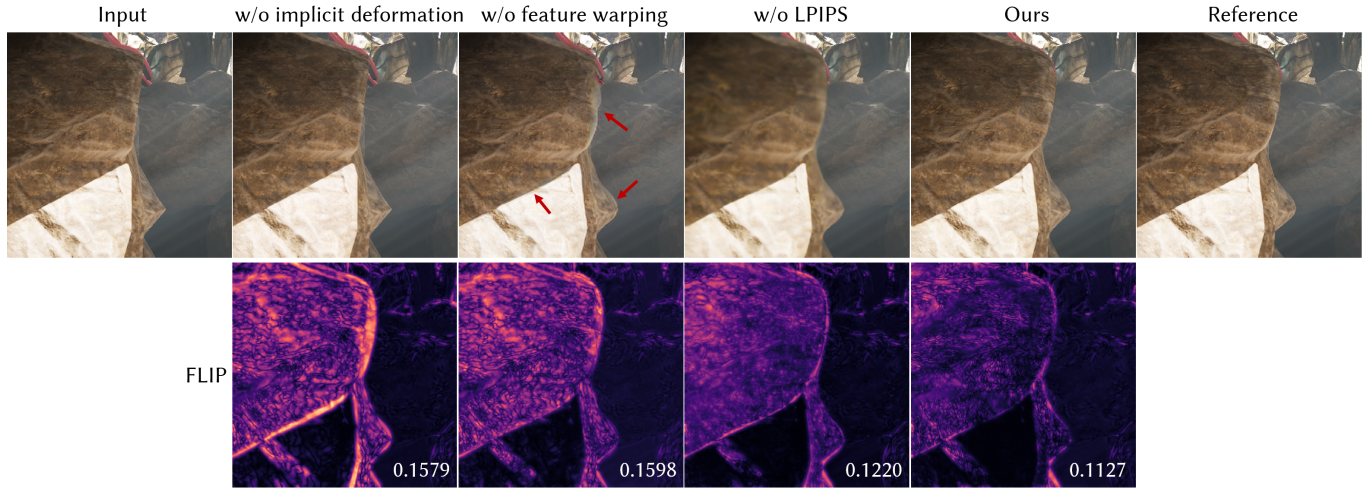


Fig. 8. Ablation study of NIST. From left to right: input rendering, variants without implicit deformation, without feature warping, without LPIPS loss, our full model, and the PN-Triangles reference. Removing the implicit deformation module prevents effective silhouette refinement. Without feature warping, visible seams and appearance discontinuities emerge in newly deformed regions (highlighted by red arrows). Excluding LPIPS leads to overly smooth and blurred results. The bottom row shows FLIP error maps with respect to the reference, where lower values indicate better perceptual similarity.

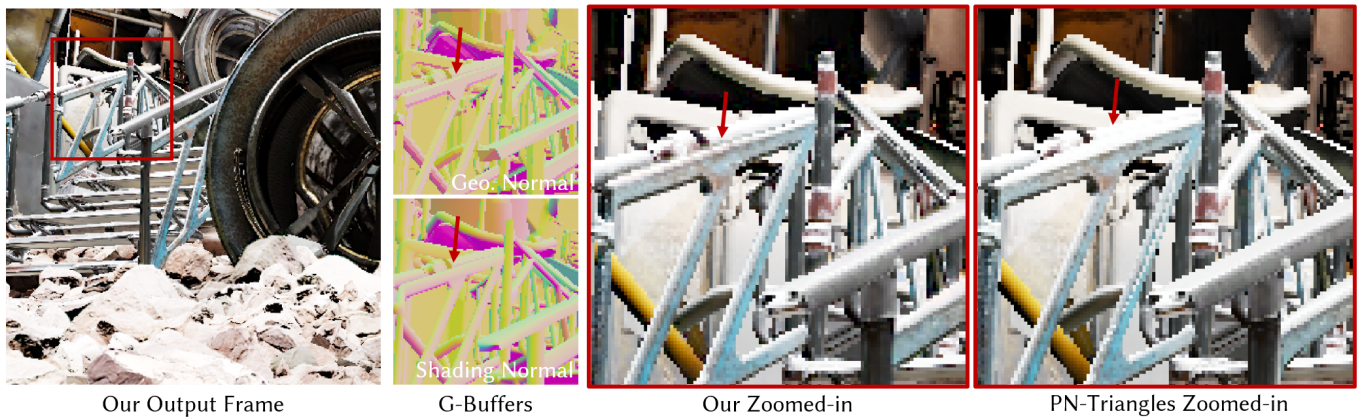


Fig. 9. Preservation of straight element guided by normal consistency. In regions where geometric normals and shading normals agree (middle), NIST correctly avoids deformation and preserves straight structures (left, zoom-in), while PN-Triangles introduces undesired deformation (right, zoom-in).